From laterally modulated two-dimensional electron gas towards artificial graphene

2012 New J. Phys. 14 053002

(http://iopscience.iop.org/1367-2630/14/5/053002)

New Journal of Physics
The open-access journal for physics

From laterally modulated two-dimensional electron gas towards artificial graphene

L Nádvorník[1,2,7], M Orlita[1,2,3], N A Goncharuk[4], L Smrčka[2], V Novák[2], V Jurka[2], K Hruška[2], Z Výborný[2], Z R Wasilewski[5], M Potemski[3] and K Výborný[2,6]

[1] Faculty of Mathematics and Physics, Charles University, Ke Karlovu 3, 121 16 Praha 2, Czech Republic
[2] Institute of Physics, ASCR, v.v.i., Cukrovarnická 10, 162 53 Praha 6, Czech Republic
[3] Laboratoire National des Champs Magnétiques Intenses, CNRS-UJF-UPS-INSA, 25, avenue des Martyrs, 38042 Grenoble, France
[4] ABB s.r.o., Semiconductors, R&D, Novodvorska 1768/138a, 14221 Prague, Czech Republic
[5] Institute for Microstructural Sciences, National Research Council of Canada, Ottawa, ON, K1A 0R6, Canada
[6] Department of Physics, University at Buffalo–SUNY, Buffalo, NY 14260, USA
E-mail: nadvl@fzu.cz

New Journal of Physics **14** (2012) 053002 (16pp)
Received 28 December 2011
Published 1 May 2012
Online at http://www.njp.org/
doi:10.1088/1367-2630/14/5/053002

Abstract. Cyclotron resonance has been measured in far-infrared transmission of GaAs/$Al_xGa_{1-x}As$ heterostructures with an etched trigonal lateral superlattice intended to mimic graphene with lattice constant of the order of 100 nm (about 1000 times larger than that of natural graphene). Nonlinear dependence of the resonance position on magnetic field was observed, as well as its splitting into several modes. Our explanation, based on a perturbative calculation, describes the observed phenomena as a weak effect of the lateral potential on the two-dimensional electron gas. Using this approach, we found a correlation between parameters of the lateral patterning and the created effective potential and obtained thus insights into how the electronic miniband structure has been tuned. The miniband dispersion was calculated using a simplified model and allowed us to formulate four basic criteria that have to be satisfied to reach graphene-like physics in such systems.

[7] Author to whom any correspondence should be addressed.

Contents

1. Introduction

The range of approaches to explore Dirac fermions in condensed-matter physics has recently been extended beyond natural graphene [1–3] to artificially created lattices whose properties such as inter-site coupling or lattice constant can be tuned. One approach here is to subject the gas of ultracold atoms to a honeycomb optical lattice [4] giving rise to Dirac cones in dispersion relations [5, 6]. The same has been proposed for lithographically patterned two-dimensional electron gases (2DEGs) in semiconductor heterostructures [7–9] as shown in figure 1. Apart from studying the Dirac fermions on their own, an appealing perspective in such semiconductor-based systems would be to fabricate various proof-of-principle electronic devices originally proposed for natural graphene [10], for instance filters and valves [11], Veselago lenses [12] or splitters [13]. The electron-beam lithography used to define the artificial honeycomb crystal potential, dubbed artificial graphene (AG) [9], allows for much easier control over the device details such as the edge geometry, additional or missing 'atoms' compared to atom-by-atom manipulation [14] in the case of natural graphene.

The subject of this paper, the fabrication and theoretical description of AG, represents a special case of lateral semiconductor superlattices (SLs) intensively studied especially in 1990s. The body of widely explored phenomena can be roughly divided into two classes: classical and quantum-mechanical. Magneto-plasmons in far-infrared transmission [15] and commensurability oscillations [16] in a modulated 2DEG can be largely explained without invoking quantum mechanics [17, 18]. On the other hand, SLs under strong magnetic fields, which leads to magnetic breakdown [19, 20], as well as other more complex systems [21–23], require quantum-mechanical ingredients (Bohr–Sommerfeld quantization and tunnelling between semiclassical orbits).

In this context, the Dirac cone in the AG spectrum is a delicate quantum-mechanical feature just as the Hofstadter butterfly [24]—Landau bands emerging when p quanta of magnetic flux pierce q elementary cells of a square SL [25, 26]. Despite promising recent progress [9, 27, 28],

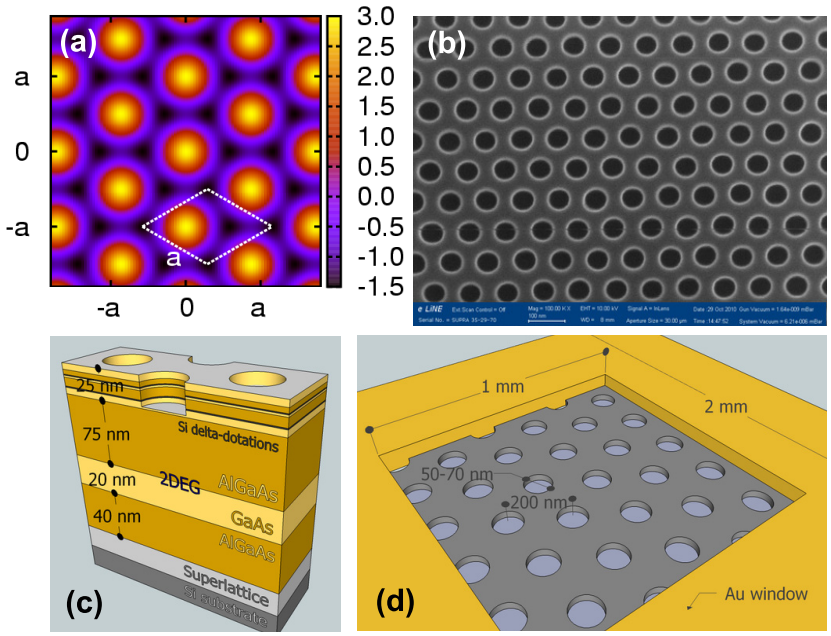

Figure 1. AG: (a) hexagonal potential of equation (1) defining the AG (in units of V_0). Dark regions correspond to carbon atoms in the real graphene lattice; the primitive cell is indicated. (b) Scanning electron microscope image of the surface of one of the samples, (c) its atomic layer structure (2DEG depth ≈ 100 nm) and (d) the sample layout (not to scale).

clear-cut evidence of Dirac fermions in AG is not yet available. Most likely, such evidence can be provided in a magneto-transport or magneto-optical experiment by observing the half-integer quantum Hall effect [1, 2], or the unique $\sqrt{B}$ scaling in the optical response due to inter-Landau level (inter-LL) transitions [29–31]. More careful engineering of AG structures is likely needed to realize these experiments.

In this paper, we explore the concept of AG both experimentally and theoretically. We use a simplified model of AG to formulate four straightforward criteria that must be fulfilled to achieve graphene-like physics in conventional 2D semiconductor heterostructures. Among these criteria, we focus on the formation of a suitable miniband structure, explain how it is related to the modulation potential amplitude and show how this quantity can be measured in far-infrared magnetotransmission. Although the Dirac fermion physics in modulated semiconductor heterostructures has not been detected so far (including the experiments presented here), we conclude that simultaneous fulfilment of all four criteria should be technologically feasible.

2. Theory

2.1. One-parametric model of artificial graphene

To arrive at transparent conditions necessary for the realization of Dirac fermions in the SL miniband structure, we use a maximally simplified AG model which is effectively single-parametric. Some previous calculations [8, 9] used muffin-tin potential whose parameters are

at minimum three: antidot distance, size and depth. A realistic form of the potential in an experimental sample is naturally hard to ascertain in detail; hence the advantage of the present model is that it is both generic and simple, single-parametric, allowing us to classify types of miniband structures that may arise while not compromising the model validity. The lesson from studies with muffin-tin potential, however, is that higher harmonics added to $V(\vec{r})$ do not ruin the Dirac cones by opening gaps, provided such additional terms preserve the honeycomb symmetry[8]. Similarly, electron–electron interactions have been shown to preserve the Dirac cones [32].

The modulation potential $V(\vec{r})$, $\vec{r} = (x, y)$, shown in figure 1(a) is taken as a sum of three cosine functions

$$V(\vec{r}) = V_0(\cos \vec{g}_1\vec{r} + \cos \vec{g}_2\vec{r} + \cos \vec{g}_3\vec{r}), \tag{1}$$

where $\vec{g}_1 = 2\pi/a(1/\sqrt{3}, 1)$, $\vec{g}_2 = 2\pi/a(2/\sqrt{3}, 0)$, $\vec{g}_3 = \vec{g}_2 - \vec{g}_1$ are the basis vectors in reciprocal space, a is the distance between two maxima of $V(\vec{r})$ and V_0 is the potential amplitude. Let us note that V_0 has to be positive to obtain a honeycomb structure rather than a trigonal one. The Hamiltonian $\hat{p}^2/2m^* + V(\vec{r})$ in basis $\mathcal{B}$ of plane waves,

$$\mathcal{B} = \left\{ e^{i(\vec{k}+\vec{K}_{n_1n_2})\vec{r}},\ \vec{K}_{n_1n_2} = n_1\vec{g}_1 + n_2\vec{g}_2 \right\}, \tag{2}$$

is a matrix whose diagonal and off-diagonal matrix elements stand in a ratio determined by V_0, a and the electron effective mass m^* (in GaAs, 0.067 of the electron vacuum mass m_0; $\hat{p}$ is the 2D momentum operator). Except for an overall scaling, eigenvalues of the matrix depend on a single dimensionless parameter

$$\zeta = \frac{m^*}{(2\pi\hbar)^2} V_0 a^2. \tag{3}$$

This parameter is, up to a factor of the order of unity, equal to the ratio between V_0 and the kinetic energy E_0 of a free electron ($V_0 = 0$) at the K-point ($\vec{K} = 2\pi/a(1/\sqrt{3}, 1/3)$) of the Brillouin zone.

Depending on ζ, we obtain miniband spectra that continuously vary from the free 2DEG, through nearly free and more tight-binding-like models, up to nearly flat bands that correspond to practically isolated (artificial) atoms. This is illustrated in figure 2, where we plot miniband structure for four different values of ζ. In figure 2(a), we plot the parabolic dispersion of a free electron ($\zeta = 0$) folded into the newly created Brillouin zone and then follow the evolution of the miniband structure with increasing ζ, namely for $\zeta = 0.3$, 0.9 and 4.0. The present Dirac cones are marked by vertical arrows and their pseudorelativistic character has been confirmed by analysing the corresponding wavefunctions[9].

Importantly, more than one Dirac cone appears within the seven lowest-lying minibands shown in figure 2. This fact, which to the best of our knowledge has so far not been mentioned in the literature, may significantly simplify the quest for pseudorelativistic physics as we discuss below. The Fermi velocity corresponding to the lower and upper Dirac cones for the modulation strength $\zeta = 0.9$ (figure 2(c)) is roughly 1.4×10^4 and 3.6×10^4 m s^{-1}, respectively. The expected Fermi velocity in AG is thus more than an order of magnitude lower as compared

[8] We thank Rafał Oszwałdowski for his comments on this topic.

[9] Evolution of wavefunctions (modulus square) upon moving on a small circle in momentum space around the K-point was studied. Degenerate-level perturbative results [8] were recovered for both Dirac cones even in the presence of mixing to levels far from the cones.

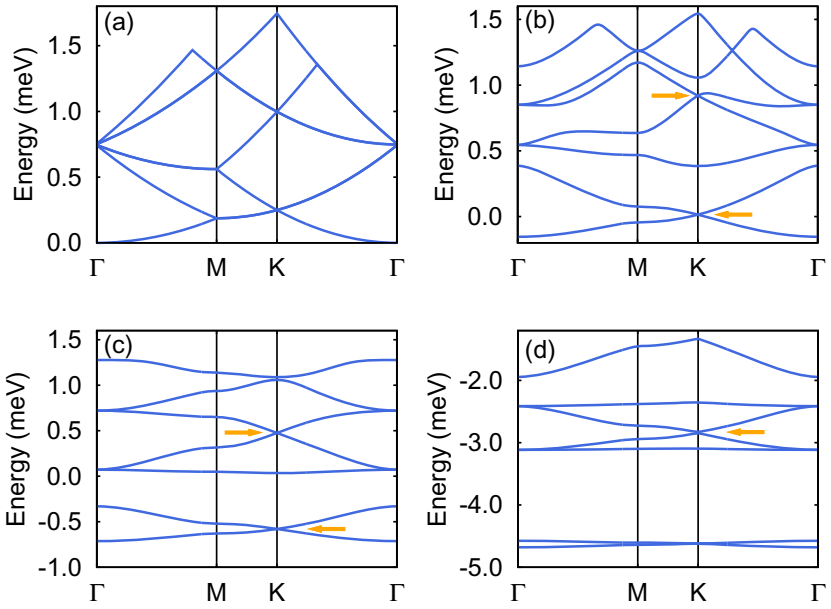

Figure 2. Minibands generated for several values of the parameter ζ. (a) $\zeta = 0$, dispersion of a free 2DEG. (b) $\zeta = 0.3$, the lower Dirac cone develops (indicated by arrows) and the upper one appears but remains covered by other bands. (c): $\zeta = 0.9$, both Dirac cones fully developed. (d) $\zeta = 4.0$, tight-binding-type narrow minibands form and Dirac cones gradually flatten, ultimately becoming again unobservable. The energy axis corresponds to GaAs effective mass and $a = 200$ nm; panels (a), (b), (c) and (d) then correspond to $V_0 = 0.0$, 0.4, 1.0 and 4.5 meV, respectively.

with natural graphene, where values around $10^6\,\mathrm{m\,s^{-1}}$ are reported [1]. Another important characteristic of the created Dirac cones is their width in energy E_{DC}. A closer inspection of figure 2 reveals that we always get the E_{DC} smaller than E_0 and also that E_{DC} strongly depends on ζ. The typical width of Dirac cones, E_{DC}, is dominantly given by two factors: the size of the Brillouin zone (i.e. the lattice constant a) and the effective mass of the employed semiconductor system (which defines the kinetic energy E_0).

2.2. *Criteria*

Now we formulate four simple criteria which have to be fulfilled to achieve Dirac-like AG physics in heterostructures subject to hexagonal modulation potential. Unless stated otherwise, we always consider lattice period $a = 200$ nm and the effective mass of electrons in GaAs $m = 0.067m_0$, which match the samples explored experimentally below.

(i) Suitable miniband structure. The effective strength of the modulation ζ has to be tuned to get well-separated and well-developed Dirac cones. Consistently with our calculations in figure 2, the range $0.5 < \zeta < 4.0$ ensures that the Dirac cones do not overlap with other minibands, as is the case for low ζ in figure 2(b), and also the cones are not significantly flattened, which gradually happens for $\zeta > 4$ towards the limit of isolated 'atoms'. If we strictly limit ourselves to the upper Dirac cone, the effective strengths ζ somewhat exceeding 4 are still acceptable. Let us note that the chosen range of ζ corresponds to the potential modulation V_0 that

ranges from 0.6 to 4.5 meV. This range will be modified by electron–electron interactions [32] and deviations of $V(\vec{r})$ from the form of equation (1); nevertheless, it may still be taken as a reasonable guide.

(ii) Fermi level positioning and/or carrier density. The Fermi level has to be located in the vicinity of a developed Dirac cone. If it is well separated from other minibands as required by the previous point, the corresponding carrier density is easy to estimate. The number of states per unit area in one miniband is equal to $4/(\sqrt{3}a^2)$ with the spin degeneracy included. The carrier density then reaches $n \approx 6 \times 10^9$ and $2.5 \times 10^{10}\,\mathrm{cm}^{-2}$ with the Fermi level located at the Dirac point of the lower and upper cones, respectively. If experiments at extremely low densities (below $10^{10}\,\mathrm{cm}^{-2}$) have to be avoided, we should preferentially focus on the upper Dirac point. Another way, if technologically feasible, is to reduce the lattice constant. For instance, $a = 100\,\mathrm{nm}$ implies a very reasonable carrier density of $1.0 \times 10^{11}\,\mathrm{cm}^{-2}$ for the upper cone. As explained above, the miniband structure for such a reduced lattice constant remains unchanged (after rescaling the energy axes in figure 2 by a factor of 4), provided V_0 is increased to keep ζ constant.

(iii) Low disorder. The idealized miniband structure, as presented in figure 2, is in reality smeared out by disorder. The minimal requirement is to have the electron mean free path $l_\mathrm{e} = \hbar\mu\sqrt{2\pi n/e^2}$ significantly exceeding the lattice constant a. For 2DEG with density of $n = 10^{11}\,\mathrm{cm}^{-2}$ and relatively low mobility $\mu = 10^5\,\mathrm{cm}^2\,(\mathrm{V\,s})^{-1}$, the mean free path reaches $l_\mathrm{e} \approx 500\,\mathrm{nm}$ and remains well above the technologically achievable a. We emphasize that this is a necessary but not a sufficient condition. This criterion becomes even more difficult to satisfy if we attempt to fabricate devices made of AG. In the structures mentioned in the introduction, there will be $\simeq 100$ lattice unit cells along the direction of Dirac fermion propagation or more; hence, the required mobilities will likely move towards current technological limits.

(iv) Careful probing. A clear piece of evidence for the presence of massless particles will likely come from experiments performed in magnetic fields, using transport [1, 2] or optical [29–31] methods. The characteristic spacing of LLs, given by the applied magnetic field B and by the effective Fermi velocity in AG, then should not exceed the Dirac cone width E_DC. This condition turns out to be numerically close to the requirement that the spacing of LLs in an unpatterned 2DEG, $\hbar\omega_\mathrm{c} = \hbar eB/m^* \approx 2 \times B[\mathrm{T}]\,\mathrm{meV}$, be small in comparison to the modulation potential V_0 and the width of the particular Dirac cone in AG, $\hbar\omega_\mathrm{c} \ll E_\mathrm{DC}$. Tolerable magnetic fields are thus hundreds of millitesla, since E_DC reaches about 1 meV at most in technologically achievable structures. Such a low magnetic field requires high-quality 2DEG samples. If we express this quality in terms of mobility, $\mu B \gtrapprox 1$. It is also important to keep temperatures low, $kT \ll \hbar\omega_\mathrm{c}$, which implicates experiments in the sub-kelvin range for realistic AG structures.

3. Experiment

3.1. Technological approaches to modulation

Lateral modulation of the 2DEG is typically achieved either by a patterned metallic layer [33, 34] used as a gate or by etching the sample surface using methods with high spatial resolution [9, 15, 25, 35, 36]. We chose the latter approach and below we comment on this choice as well as review some alternatives.

Interface effects. Mechanical strain due to lattice constants mismatch can give rise to 2DEG modulation via piezoelectric effect if we deposit a mismatching material on top of the heterostructure [38, 39]. Moreover, one can take advantage of different thermal dilatation in the two mismatching materials and thus control the modulation strength. Another option is to engineer Schottky barriers on the heterostructure surface by depositing a (patterned) metallic layer [37].

Passive electrostatic structures. If we etch out an array of dots or antidots on the surface [40], there are two mechanisms how the electron density may become altered. When the heterostructure contains donor layer(s) between the surface and the 2DEG, the etched holes remove a part of the charged donor layer and thus modify electrostatics of the surroundings. At the same time, by moving the surface closer to the 2DEG, the electrons become increasingly depleted by surface states. Moreover, the number of these surface states may be increased by the etching. An especially strong modulation can be achieved by etching through the 2DEG layer. Such structures, with regions fully depleted from electrons [17], have been mostly used to study magneto-plasmon effects [15]. On the other hand, quantum effects due to miniband structure are typically studied in shallow-etched samples [25] such as are the subject of our study. We remark that at a given pitch between dots/antidots, the antidot design allows us to get a factor of $\sqrt{3}$ lower lattice constant of AG as compared to an array of dots.

Active electrostatic elements. Gating is probably the most complex approach to tune and control the required potential [34, 41]. More sophisticated and promising concepts, such as the control of both modulation potential amplitude and carrier density, can be designed using both front and back gates. The front gate is then, for instance, a metal plate with hexagonally ordered long needles touching the heterostructure (or an oxide layer on its top). While the front gate creates an easily tunable electrostatical field, the back gate controls the actual density of carriers.

Although gating seems most promising (it allows us to tune our system to meet criteria (i) and (ii) and is likely to do reasonably well with (iii)), it is also technologically more challenging and makes our optical measurements difficult. We chose 'hole drilling' as the relatively simplest technique and consider using a back gate as the simplest way to deal with criterion (ii) in the future.

3.2. Samples and setup

The studied samples have been prepared by etching a shallow array of holes (i.e. antidots) with a triangular symmetry. Electron beam lithography and the dry etching process ($Ar^+ + SiCl_4$) have been employed. We prepared three samples denoted as A, B and C, see table 1, with the etching depths of 15–25, 20 and 48 nm, respectively. The diameter of holes was always ≈ 60 nm and the hole-to-hole distance, i.e. our AG lattice constant, $a = 200$ nm. Samples A and B have been prepared from a wafer with 2DEG in a 20 nm wide quantum well embedded between $Al_{0.33}Ga_{0.67}As$ barriers and located 100 nm below the surface. The electrons in the well are provided by two δ-doped Si layers, 15 nm (3×10^{12} cm^{-2}) and 25 nm (2×10^{12} cm^{-2}) deep, see figure 1(c). The sample C was fabricated from a simple GaAs/$Al_{0.33}Ga_{0.67}As$ heterojunction located 115 nm below the sample surface. The triangular well formed at the interface was filled by electrons from a Si-doped $Al_{0.33}Ga_{0.67}As$ region (1.5×10^{18} cm^{-3}) separated from the interface by a spacer 25 nm wide. For all three samples, the lithographically patterned area

Table 1. Potential amplitude V_0 and the corresponding dimensionless parameter ζ for samples A, B and C as derived by fitting our data using equation (7), see the text for details. The etching depths and the 2DEG-to-surface distances are also listed.

Sample	d_{holes} (nm)	d_{2DEG} (nm)	V_0 (meV)	ζ
A	15–25	100	2.2	2.0
B	20	100	3.5	3.1
C	48	115	4.0	3.6

($1 \times 1\,\text{mm}^2$) was surrounded by a gold frame (50 nm thick) to define the optically active part for the transmission experiment, see figure 1(d).

The prepared samples have been studied using the infrared magneto-spectroscopy technique, in this case having the form of the LL spectroscopy. To measure the magneto-transmission of the sample, the radiation of the globar or mercury lamp was modulated by a Fourier transform spectrometer. We worked with photon energies down to 4 meV at a resolution of 0.125 meV. The radiation was delivered via light-pipe optics to the sample kept at 2 K inside a superconducting coil and detected by a Si bolometer, placed directly below the sample. All measurements were carried out in the Faraday configuration with the magnetic field applied perpendicular to the sample layer.

3.3. Results

Characteristic results of the magneto-transmission experiment are presented in figure 3. Relative magneto-transmission spectra are shown, i.e. for each photon energy, the transmission at a given field normalized to the same at $B = 0\,\text{T}$. A well-defined CR absorption of a nearly Lorentzian shape is obtained for all three samples at higher magnetic fields. When the magnetic field is lowered, we observe more complex behaviour with the CR absorption split into two or even more modes. The energy distance between these modes is clearly different in various samples and it is correlated with the depth of the etched holes, i.e. with the strength of the modulation potential induced by the lateral patterning. An unpatterned reference sample, taken from the wafer used for fabrication of samples A and B, has also been tested. As expected, it showed a typical Lorentzian-shaped CR absorption at the energy of $\hbar\omega_c$ in the entire available range of magnetic fields.

Since the initial carrier concentration in the dark was or could be modified during technological processing and also, since the carrier concentration is affected by the near-infrared part of the globar/mercury lamp radiation (due to persistent photoconductivity), we estimated the carrier densities directly from the strength of CR [42]. This analysis has been performed at higher fields, when all specimens provide a well-defined CR absorption of Lorentzian shape. The evaluated densities for samples A, B and C are $n_{\text{A,B}} \sim 0.7 \times 10^{11}\,\text{cm}^{-2}$ and $n_{\text{C}} \sim 1.8 \times 10^{11}\,\text{cm}^{-2}$, respectively. Optionally, this density could be further increased by illumination with an infrared diode. Using the CR absorption width, we roughly estimated also the carrier mobility in samples after processing, which was found to be somewhat in excess of $10^5\,\text{cm}^2\,(\text{V s})^{-1}$ for all three specimens.

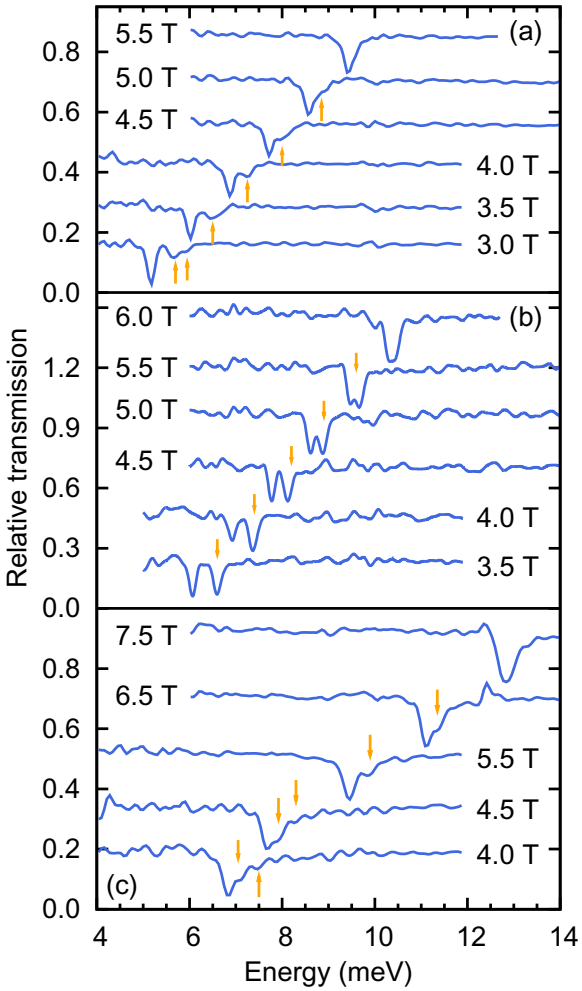

Figure 3. Relative magneto-transmission spectra of studied samples A ($d_{\text{holes}} \approx$ 15–25 nm, $d_{\text{2DEG}} = 100$ nm), B ($d_{\text{holes}} = 20$ nm, $d_{\text{2DEG}} = 100$ nm) and C ($d_{\text{holes}} =$ 48 nm, $d_{\text{2DEG}} = 115$ nm) in panels (a), (b) and (c), respectively. The multi-mode character of cyclotron resonance (CR) absorption vanishes above $B \approx 5$, 6 and 7 T in samples A, B and C, respectively. All spectra are shifted vertically for clarity.

4. Interpretation

The observed departure from a single-mode CR at energy $\hbar\omega_c$ shows a clear effect of the lateral modulation and we discuss two possible scenarios to interpret this finding. The first one relies on a quantum-mechanical (single-particle) approach and assumes the AG miniband structure due to the lateral periodic potential. These minibands are transformed into dispersively broadened LLs at nonzero magnetic field. The second scenario, a classical one, recalls characteristic multimode CR absorption observed in systems dominated by (confined) magneto-plasmons. We commence our discussion by showing that this latter scenario is, if considered in detail, inconsistent with our measurements.

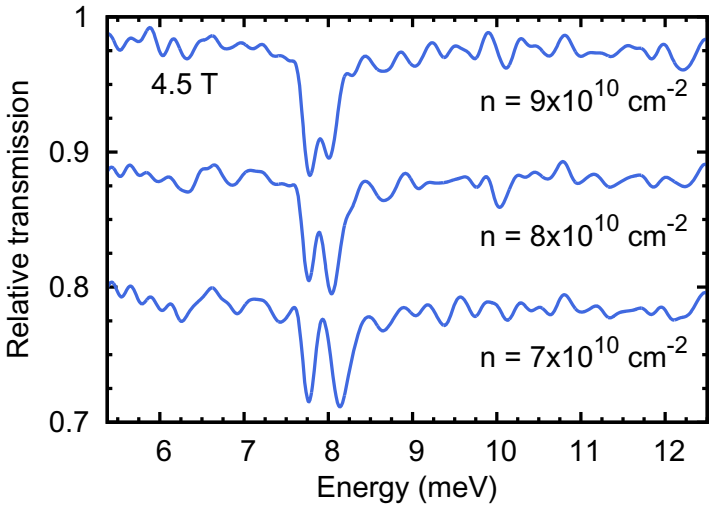

Figure 4. Magneto-transmission spectra (shifted vertically for clarity) taken on sample B at $B = 4.5$ T with three different carrier concentrations adjusted by gradually increasing the illumination time. Splitting of the observed modes clearly decreases with increasing carrier density.

4.1. Confined magneto-plasmons

Splitting of the CR absorption in diminishing magnetic fields, as shown in figure 3, is reminiscent of magneto-plasma oscillations in a 2DEG [45]. Indeed, the magneto-optical response of our samples, which consists of a basic CR absorption line accompanied by one or more modes at (only) higher energies, resembles spectra taken on a 2DEG with 1D lateral modulation or on a confined unmodulated 2DEG (stripe) [46–48]. Let us therefore compare our results to the response of magneto-plasmons in a 2DEG subject to lateral modulation in both directions, in particular in antidot lattices [15, 49]. In such a case, the far-infrared or microwave magneto-absorption response includes, among others, a characteristic lower branch located below the CR energy, which is well documented experimentally and explained theoretically [40]. This lower branch is interpreted as an edge-magneto-plasmon (EMP), circulating around the antidot, and its existence is not directly connected with the symmetry of the antidot lattice [17, 50].

No sign of any EMP mode below CR energy has been observed in our experiments. We take this as a clear argument against the interpretation of the observed multi-mode CR response in terms of magneto-plasmons. Another test to exclude magneto-plasmon effects was performed using external illumination with an infrared diode. Upon a gradual increase of the carrier density n in sample B (as evidenced by the strength of the CR absorption at high magnetic fields), the distance of observed modes shown in figure 4 decreased with n. For magneto-plasmonic excitations, an opposite trend is expected [49]. We also recall that the experiment of K Ploog's group [15] concerned deeply etched samples and that magneto-plasmon behaviour has been typically detected at significantly higher densities.

4.2. Analysis with respect to criterion (i)

We now turn to a discussion of the experimental facts with respect to the four criteria to observe massless Dirac fermions in a laterally modulated 2DEG. This provides us with basic estimates

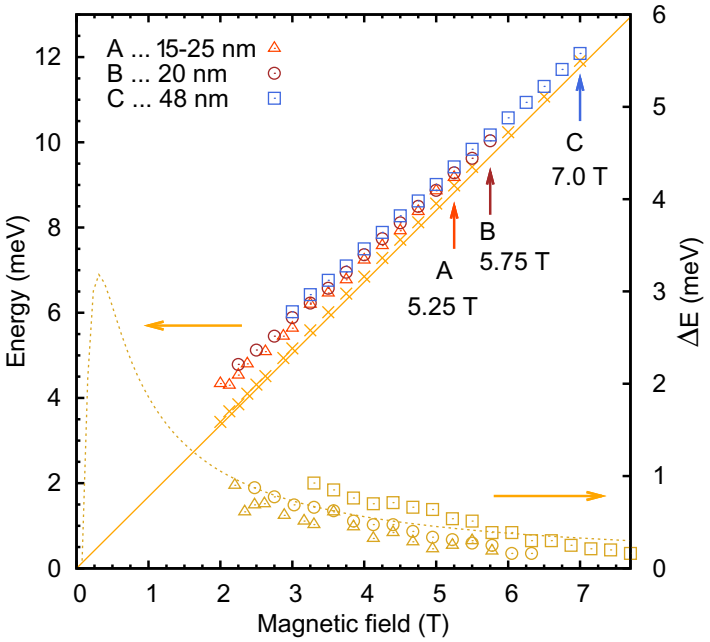

Figure 5. Transitions observed in specimens A, B and C, compare to figure 3 (left vertical axis; depths of etched holes are indicated). Vertical arrows indicate magnetic fields at which the multi-mode character of CR absorption vanishes. The position of the main CR peak in spectra taken on sample A is marked by crosses. The straight line corresponds to the theoretical CR-line position with an effective mass of $m^* = 0.067m_0$, which has been derived from measurements on reference (unpatterned) sample (not shown). Lower part of the figure (right vertical axis) shows determined values of the CR-line splitting ΔE. The dashed line corresponds to the fit of ΔE for the sample A based on the theoretical model discussed in the text.

on how close or far we are from Dirac-like conditions. These criteria, formulated in section 2, are related to the (mini)band electronic structure, carrier density, disorder in the system and also to the chosen experimental technique and conditions. We first discuss criterion (i) for which we need an estimate of the modulation potential amplitude V_0. We show that infrared magneto-spectroscopy is a method suitable for this purpose.

The main absorption features in figure 3 occur close to $\hbar\omega_c$ but in contrast to the CR of an unmodulated 2DEG, they have an internal structure which disappears roughly as $1/B$ (see figure 5) in the limit of high magnetic fields. Such behaviour suggests that the influence of the modulation potential becomes gradually weaker with increasing B and potential energy $V(\vec{r})$ acts as a perturbation to the LLs. Their spacing, the cyclotron energy $\hbar\omega_c$, then provides the dominant energy scale compared to the modulation potential V_0 and the small parameter is $V_0/\hbar\omega_c \propto 1/B$. In the first-order perturbation calculation [43], the unperturbed energies $E_n = \hbar\omega_c(n + 1/2)$ become broadened into bands:

$$E_{n,\kappa_x,\kappa_y} = E_n + V_0\, \mathrm{e}^{-2\beta^2/3} L_n(4\beta^2/3) \left\{ 2\cos\beta^2(\kappa_x + \tfrac{1}{\sqrt{3}}) \cos\frac{\beta^2\kappa_y}{\sqrt{3}} + \cos\frac{2\beta^2\kappa_y}{\sqrt{3}} \right\}, \tag{4}$$

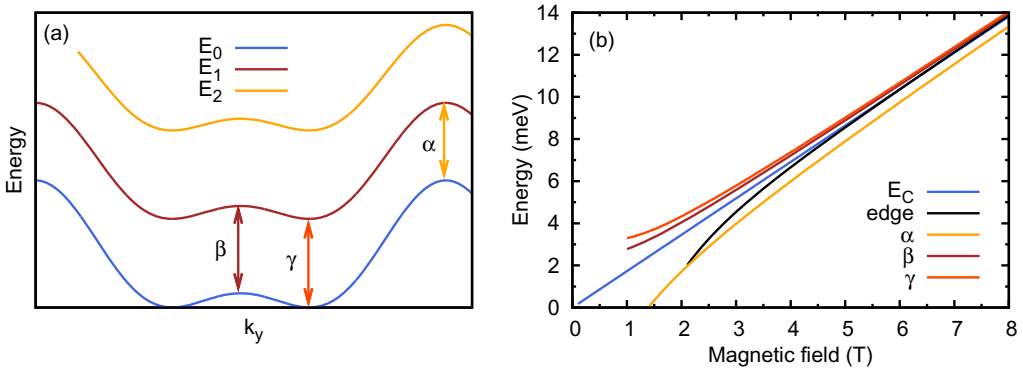

Figure 6. (a) Schematic plot of three lowest-lying LLs broadened into bands due to the lateral hexagonal modulation. Transitions related to the van Hove singularities in the joint density of states (jDOS) $a(\omega)$ are marked by α, β and γ. Whereas α and γ are the band edges, β is the logarithmic singularity corresponding to the saddle point between two neighbouring minima of ΔE_{10} in $\vec{\kappa}$-space. (b) Magnetic field dependence of jDOS α, β, γ singularity positions. 'Edge' shows the lowest in energy allowed transition, as defined by the position of the Fermi level (for $n = 1.0 \times 10^{11}$ cm^{-2}). $E_c = \hbar\omega_c$ is the cyclotron energy.

where $\beta^2 = 2\pi^2\ell_0^2/a^2$, $\ell_0^2 = \hbar/eB$ and $\vec{\kappa}$ belongs to the hexagonal first magnetic Brillouin zone. Owing to the special properties of Laguerre polynomials L_n [44], optical transition energies, $E_{n+1,\kappa_x,\kappa_y} - E_{n,\kappa_x,\kappa_y}$, can be rewritten in a simple way. Since we deal with low carrier concentrations at which only the lowest LL is occupied, we can restrain ourselves to $n = 0$,

$$\Delta E_{1,0} = E_{1,\kappa_x,\kappa_y} - E_{0,\kappa_x,\kappa_y} = \hbar\omega_c - \tfrac{4}{3}V_0\beta^2 e^{-2\beta^2/3} b(\kappa_x, \kappa_y), \tag{5}$$

where $b(\kappa_x, \kappa_y)$ denotes the curly bracket of equation (4).

The optical transition energy $\Delta E_{1,0}$ enters the absorption probability $\alpha_{1,0}$ for a photon of frequency ω that has caused a transition between $n = 0$ and $n = 1$ LLs. Provided that the former (latter) LL is full (empty), this probability is proportional to[10]

$$\int \frac{d^2\kappa}{(2\pi)^2} |\langle 1, \kappa_x, \kappa_y | p_x | 0, \kappa_x, \kappa_y \rangle|^2 \delta(\Delta E_{1,0} - \hbar\omega). \tag{6}$$

If we neglect the dipole transition matrix element (a transition between the two mentioned LLs is allowed by selection rules), the characteristic spectral features correspond to the van Hove singularities indicated in figure 6, in the occupation-weighted jDOS:

$$a(\omega) = \int \frac{d^2\kappa}{(2\pi)^2} \delta(\Delta E_{1,0} - \hbar\omega) f_{0,\kappa_x,\kappa_y}(1 - f_{1,\kappa_x,\kappa_y}),$$

in which all those transitions at a given energy $\hbar\omega = \Delta E_{1,0}$ count where the initial ($n = 0$) state is occupied and the final ($n = 1$) state is empty, as expressed by the Fermi–Dirac factors f. At a

[10] Photon absorption in a 2D SL is derived, for example, by V Demikhovskii and A Perov [52], and a more general discussion can be found on page 241 in G Bastard [53].

filling factor $\nu = nh/eB = 2$, which was assumed in expression (6), $a(\omega)$ is a band of width

$$w(B) = 6V_0\beta^2\,\mathrm{e}^{-2\beta^2/3} \tag{7}$$

situated close to $\omega = \omega_c$. The width of the band decreases with decreasing ν (at constant β), as the filling of the $n = 0$ LL decreases and smaller portions of the magnetic Brillouin zone become available for transitions. In the limit of very large B, $a(\omega)$ turns into a zero-width peak at exactly $\omega = \omega_c$.

Equation (7) provides us with a reasonable basis for the interpretation of the experimental data presented in figures 3(a)–(c). The peak-to-peak distance shown as the lower data sets in figure 5 follows the magnetic field dependence of $w(B)$ allowing us to extract the values of V_0 for the particular sample. It should be noted, however, that the peak splitting observed in experiments does not correspond to the full-width w as calculated using equation (7) because the lower edge of the absorption band is suppressed for $\nu < 2$. This is the case of $B > 2$T and $n < 10^{11}\,\mathrm{cm}^{-2}$ when spin degeneracy remains unresolved (Zeeman splitting ε_z is roughly an order of magnitude smaller than the CR peak width at $B = 2\,\mathrm{T}$; $\varepsilon_z = g_s e\hbar B/2m_0 \approx 0.06\,\mathrm{meV}$ for $|g_s| \approx 0.44$ as appropriate in GaAs systems [51]). Features of the jDOS appearing in the absorption band scale as $cw(B)$, where $0 < c < 1$ is a constant. These features are shown in figure 6 and correspond to the indicated transitions of the broadened Landau bands E_{n,κ_x,κ_y}. The first states that become depopulated upon the filling factor dropping below two (that is when the magnetic field is increased) are those close to the top of the band. Correspondingly, the transitions α are the first ones to disappear from the absorption spectra.

For the remaining two features β and γ, our form of the potential $V(x, y)$ would imply $c = 1/9$. However, since the transition β gives rise to a logarithmic singularity which is likely to be smeared out, we focus on another candidate for an absorption feature: the Fermi edge which is also shown in the right panel of figure 6 (transitions from the states close to E_F to the next Landau band). Although the Fermi edge does not precisely scale with $w(B)$, it appears at frequencies $\omega \approx \omega_c$; hence we take $c \approx 1/3$. The values of V_0 inferred from fitting our data, assuming that the splitting of the CR mode corresponds to $\frac{1}{3}w(B)$, are shown in table 1 along with the corresponding ζ. We can now return to criterion (i), and see that, as anticipated at the beginning of section 3, shallow etching may create modulation potential favourable for Dirac-fermion physics in AG as quantified by the first criterion in section 2.

4.3. Discussion of the other criteria

While criterion (i) seems satisfied for our samples, the carrier density is by a factor of ≈ 3 too large compared to the requirement (ii), even in the most favourable situation (upper Dirac cone, samples A, B). Since further lowering of n may induce metal-to-insulator transition [27] a better strategy seems to be to reduce the lattice constant. Further technological improvements will, however, then be required to keep criterion (iii) fulfilled. In our case, the measured mobility implies mean free path only a few times larger than the lattice constant and the former is likely to deteriorate rapidly upon pushing electron lithography closer to its limits of spatial resolution. Once the criteria (i)–(iii) are met for some sample, one should proceed to low-field ($B \approx 0.1$T) and low-temperature ($\lesssim 1\,\mathrm{K}$) experiments as required by the last criterion (iv). Since inter-LL transitions will then be in the sub-THz range and fabrication of samples homogeneous on a scale comparable to the wavelength of absorbed light will be difficult, magnetotransport or photoluminescence experiments seems most promising.

5. Summary and conclusions

The concept of AG has been explored both experimentally and theoretically. Based on a simple theoretical model, we formulated four basic criteria that need to be met in order to create and experimentally demonstrate the proposed graphene-like bands in modulated semiconductor heterostructures. We have prepared three samples with lateral modulation and investigated them using infrared magneto-spectroscopy. The results have been discussed with respect to the proposed criteria with the following conclusions. Etching an antidot (hole) lattice on the sample surface creates lateral modulation potential with favourable strength, which, according to our model, should give rise to a miniband structure containing well-developed Dirac cones. An empirical rule, which connects the depth of etched holes with the strength of the lateral potential, has been found for our technological protocol. The quality of prepared specimens, expressed in terms of mobility or mean free path, could be sufficient for resolving the AG electronic structure with the Dirac cones; nevertheless, further increase of this quality would be desirable. The main obstacle preventing until now the realization of Dirac-like physics in 2DEG seems to be related to the interplay between the electron density and the lattice constant. Since lowering the carrier density down to the $10^9\,\mathrm{cm}^{-2}$ range seems unrealistic, we instead logically suggest to reduce the lattice constant below 100 nm. This is technologically challenging, given the constraints on mobility, but nevertheless feasible. Furthermore, we propose to focus on a higher Dirac cone, which is found in an AG miniband structure and which could be probed at higher carrier densities, namely at $n \approx 10^{11}\,\mathrm{cm}^{-2}$ for $a = 100$ nm. With these suggestions, we believe that massless Dirac fermions can be observed in laterally modulated 2DEG, probably using infrared or THz magneto-spectroscopy or the magneto-transport technique, in the (possibly not too distant) future.

Acknowledgments

The authors thank P Hubík and J Čermák for technological assistance and J Wunderlich for valuable critical remarks. Moreover, support from the following institutions is acknowledged: the Ministry of Education via the Czech Republic projects LC510 and IRMA, GAČR through grant no. P204/10/1020, the Charles University in Prague via grants GAUK No. 425111 and SVV-2011-263306, the Academy of Sciences of the Czech Republic via Institutional Research Plan no. AV0Z10100521, KAN 400100652, GAAV contract KJB100100802, Præmium Academiæ, Fondation *NanoScience* via the project Dispograph, overseas funding bodies via NSF-NRI NEB 2020 and SRC and, last but not least, EC-EuroMagNetII under contract no. 228043.

References

[1] Novoselov K S, Geim A K, Morozov S V, Jiang D, Katsnelson M I, Grigorieva I V, Dubonos S V and Firsov A A 2005 *Nature* **438** 197
[2] Zhang Y B, Tan Y W, Stormer H L and Kim P 2005 *Nature* **438** 201
[3] Geim A K and Novoselov K S 2007 *Nature Mater.* **6** 183
[4] Grynberg G, Lounis B, Verkerk P, Courtois J-Y and Salomon C 1993 *Phys. Rev. Lett.* **70** 2249
[5] Zhu S-L, Wang B and Duan L M 2007 *Phys. Rev. Lett.* **98** 260402

[6] Wunsch B, Guinea F and Sols F 2008 *New J. Phys.* **10** 103027
[7] Park C H, Yang L, Son Y W, Cohen M L and Louie S G 2008 *Phys. Rev. Lett.* **101** 126804
[8] Park C H and Louie S G 2009 *Nano Lett.* **9** 1793
[9] Gibertini M, Singha A, Pellegrini V, Polini M, Vignale G, Pinczuk A, Pfeiffer L N and West K W 2009 *Phys. Rev.* B **79** 241406
[10] Dubois S M-M, Zanolli Z, Declerck X and Charlier J-C 2009 *Eur. Phys. J.* B **72** 1
[11] Rycerz A, Tworzydło J and Beenakker C W J 2007 *Nature Phys.* **3** 172
[12] Cheianov V V, Fal'ko V and Altshuler B L 2007 *Science* **315** 1252
[13] Garcia-Pomar J L, Cortijo A and Nieto-Vesperinas M 2008 *Phys. Rev. Lett.* **100** 236801
[14] Eigler D M and Schweizer E K 1990 *Nature* **344** 524
[15] Kern K, Heitmann D, Grambow P, Zhang Y H and Ploog K 1991 *Phys. Rev. Lett.* **66** 1618
[16] Weiss D, Klitzing K V, Ploog K and Weimann G 1989 *Europhys. Lett.* **8** 179
[17] Mikhailov S A 1996 *Phys. Rev.* B **54** R14293
[18] Beenakker C W J 1989 *Phys. Rev. Lett.* **62** 2020
[19] Středa P and MacDonald A H 1990 *Phys. Rev.* B **41** 11892
[20] Gvozdikov V M 2007 *Phys. Rev.* B **75** 115106
[21] Albrecht C, Smet J H, Weiss D, Klitzing K V, Hennig R, Langenbuch M, Suhrke M, Rössler U, Umansky V and Schweizer H 1999 *Phys. Rev. Lett.* **83** 2234
[22] Olszewski S, Pietrachowicz M and Baszczak M 2004 *Phys. Status Solidi* b **241** 3572
[23] Gvozdikov V M 2007 *Phys. Rev.* B **76** 235125
[24] Hofstadter D R 1976 *Phys. Rev.* B **14** 2239
[25] Geisler M C, Smet J H, Umansky V, Klitzing K V, Naundorf B, Ketzmerick R and Schweizer H 2004 *Phys. Rev. Lett.* **92** 256801
[26] Pfannkuche D and Gerhardts R R 1992 *Phys. Rev.* B **46** 12606
[27] Simoni G D, Singha A, Gibertini M, Karmakar B, Polini M, Piazza V, Pfeiffer L N, West K W, Beltram F and Pellegrini V 2010 *Appl. Phys. Lett.* **97** 132113
[28] Singha A *et al* 2011 *Science* **332** 1176
[29] Sadowski M L, Martinez G, Potemski M, Berger C and de Heer W A 2006 *Phys. Rev. Lett.* **97** 266405
[30] Jiang Z, Henriksen E A, Tung L C, Wang Y-J, Schwartz M E, Han M Y, Kim P and Stormer H L 2007 *Phys. Rev. Lett.* **98** 197403
[31] Deacon R S, Chuang K-C, Nicholas R J, Novoselov K S and Geim A K 2007 *Phys. Rev.* B **76** 081406
[32] Räsänen E *et al* 2012 arXiv:1201.1734
[33] Soibel A, Meirav U, Mahalu D and Shtrikman H 1996 *Semicond. Sci. Technol.* **11** 1756
[34] Hugger S, Heinzel T and Thurn-Albrecht T 2008 *Appl. Phys. Lett.* **93** 102110
[35] Takahara J, Nomura A, Gamo K, Takaoka S, Murase K and Ahmed H 1995 *Japan. J. Appl. Phys.* **34** 4325
[36] Geisler M C, Chowdhury S, Smet J H, Höppel L, Umansky V, Gerhardts R R and Klitzing K V 2005 *Phys. Rev.* B **72** 045320
[37] Kasai S and Hasegawa H 1996 *Japan. J. Appl. Phys.* **35** 1340
[38] Skuras E, Long A R, Larkin I A, Davies J H and Holland M C 1997 *Appl. Phys. Lett.* **70** 871
[39] Endo A and Iye Y 2005 *J. Phys. Soc. Japan* **74** 2797
[40] Heitmann D and Kotthaus J P 1993 *Phys. Today* **46** 56
[41] Lorke A, Jejina I and Kotthaus J P 1992 *Phys. Rev.* B **46** 12845
[42] Chiu K, Lee T and Quinn J 1976 *Surf. Sci.* **58** 182
[43] Wang X F, Vasilopoulos P and Peeters F M 2004 *Phys. Rev.* B **69** 035331
[44] Gradshteyn I S and Ryzhik I M 1980 *Table of Integrals, Series, and Products* (New York: Academic)
[45] Stern F 1967 *Phys. Rev. Lett.* **18** 546
[46] Mikhailov S A and Savostianova N A 2005 *Phys. Rev.* B **71** 035320

[47] Mikhailov S A and Savostianova N A 2006 *Phys. Rev.* B **74** 045325
[48] Fedorych O M, Studenikin S A, Moreau S, Potemski M, Saku T and Hirayama Y 2009 *Int. J. Mod. Phys.* B **23** 2698
[49] Zhao Y, Tsui D C, Santos M, Shayegan M, Ghanbari R A, Antoniadis D A and Smith T I 1992 *Appl. Phys. Lett.* **60** 1510
[50] Mikhailov S A and Volkov V A 1995 *Phys. Rev.* B **52** 17260
[51] Yugova I A, Greilich A, Yakovlev D R, Kiselev A A, Bayer M, Petrov V V, Dolgikh Yu K, Reuter D and Wieck A D 2007 *Phys. Rev.* B **75** 245302
[52] Demikhovskii V and Perov A 1998 *J. Exp. Theor. Phys.* **87** 973
[53] Bastard G 1991 *Wave Mechanics Applied to Semiconductor Heterostructures* (New York: Wiley)